0026-895X/01/5904-920–928$3.00
MOLECULAR PHARMACOLOGY
Copyright © 2001 The American Society for Pharmacology and Experimental Therapeutics
Mol Pharmacol 59:920–928, 2001

Vol. 59, No. 4
430/893401
Printed in U.S.A.

Quinazolone-Alkyl-Carboxylic Acid Derivatives Inhibit Transmembrane Ca^{2+} Ion Flux to (+)-(*S*)-α-Amino-3-hydroxy-5-methylisoxazole-4-propionic Acid

ÉVA SZÁRICS, LAJOS NYIKOS, PÉTER BARABÁS, ILONA KOVÁCS, NINA SKUBAN, ESZTER TEMESVÁRINÉ-MAJOR, ORSOLYA EGYED, PETER I. NAGY, JÓZSEF KÖKÖSI, KRISZTINA TAKÁCS-NOVÁK, and JULIANNA KARDOS

Departments of Neurochemistry (É.S., L.Y., P.B., I.K., N.S., J.Ka.) and Syntheses of Natural Organic Compounds (E.T.-M.), Optical Spectroscopy Group (O.E.), Chemical Institute, Chemical Research Center, Hungarian Academy of Sciences, Budapest, Hungary; Institute of Pharmaceutical Chemistry, Semmelweis University (J.Kö., K.T.-N.) Budapest, Hungary; and Department of Medicinal and Biological Chemistry, The University of Toledo, Toledo, Ohio (P.I.N.)

Received July 19, 2000; accepted December 19, 2000

This paper is available online at http://molpharm.aspetjournals.org

ABSTRACT

Comparison of the kinetics of the inward Ca^{2+} ion flux to (*S*)-α-Amino-3-hydroxy-5-methylisoxazole-4-propionic acid [(*S*)-AMPA] in cerebrocortical homogenates and that of the previously reported transmembrane Na^{+} ion influx mediated by an AMPA receptor in hippocampal homogenates established that the agonist-induced opening of the AMPA receptor channels occurs in two kinetically distinguishable phases. Here we report that the 2-methyl-4-oxo-3*H*-quinazoline-3-acetic acid (Q1) inhibits the major slow-phase response specifically, whereas the acetyl piperidine derivative (Q5) is a more potent inhibitor of the fast-phase response. Both the quinazolone-3-propionic acid (Q2) and the quinazolone-3-acetic acid methyl ester (Q3) enhanced the slow-phase response to (*S*)-AMPA. The information provided by docking different Q1, Q2, and Q5 models at the ligand-binding core of iGluRs were used to define agonistic and antagonistic modes of interactions. Based on the effects of quinazolone-3-alkyl-carboxylic acid derivatives on specific [^{3}H]Glu binding and kinetically distinguishable Ca^{2+} ion permeability responses to (*S*)-AMPA and molecular modeling, the fast- and the slow-phase (*S*)-AMPA-elicited Ca^{2+} ion fluxes were corresponded to different subunit compositions and degrees of S1S2 bridging interaction relative to substitution of kainate thereupon. Substitutions of agonists and antagonists into the iGluR2 S1S2 ligand binding core induced different modes of domain-domain bridging.

The seminal information on the structure of an ionotropic glutamate receptor (iGluR) in complex with the neurotoxic agonist, kainate (Armstrong et al., 1998), together with the concept of the autonomous ligand-binding core for all iGluRs (Paas, 1998), opened up the development of drugs targeting iGluR more specifically. Polar groups dock kainate at the interdomain pocket formed by two polypeptide segments, S1 and S2, via multiple interactions with the amino acid residues of the ligand-binding core. Here we describe effects of quinazolone-alkyl-carboxylic acid derivatives (QXs; Fig. 1) on the rates of transmembrane Ca^{2+} ion influx to (*S*)-AMPA. In addition, measurements on specific [^{3}H]Glu binding in rat brain cortical homogenates containing resealed plasmalemmal vesicles and nerve endings were performed to clarify the subunit compositions of receptors in the interpretation of the data as well as to justify the use of the iGluR2-S1-S2 crystal structure to model the ligand docking that modulates Ca^{2+} ion flux. We attempt, on the basis of these results, 1) to integrate kinetics, pharmacological profile, and three-dimensional structure of the receptor-ligand complex to understand the molecular features of the Glu-gated ion channel-ligand interactions, and 2) to identify prerequisites for AMPA receptor agonist and antagonist specifics, by relating results from measurements of an AMPA receptor function with the relative position of the agonist-binding-site domains.

Experimental Procedures

Materials. Male Wistar rats (3–6 weeks old) purchased from Toxicoop (Budapest, Hungary) were kept and used in accordance

ABBREVIATIONS: iGluR, ionotropic glutamate receptor; kainate, [2*S*-(2α,3β,4β)]-2-carboxy-4-(1-methylethenyl)-3-pyrrolidineacetic acid; AMPA, α-amino-3-hydroxy-5-methylisoxazole-4-propionic acid; bisFURA2, 1,2-bis-[2-(carboxyoxazole-2-yl)-6-aminobenzofuran-5-oxy]-ethane-*N*,*N*,*N*′,*N*′-tetraacetic acid hexa-potassium salt; *t*ACPD, (1*S*,3*R*)-1-aminocyclopentane-1,3-dicarboxylic acid; CNQX, 6-cyano-7-nitroquinoxaline-2,3-dione; cyclothiazide, 6-chloro-3,4-dihydro-3-(2-norbornen-5-yl)-2*H*-1,2,4-benzothiadiazine-7-sulfonamide-1,1-dioxide, MK-801, 5-methyl-10,11-dihydro-5*H*-dibenzo[*a*,*d*]cycloheptene-5,10-imine maleate; QX, Quinazolone-3-alkyl-carboxylic acid derivative [Q1, acetic acid; Q2, propionic acid; Q3, methylacetate; Q4, diethylacetamide; Q5, acetyl piperidine; Q6, acetyl morpholine]; NPMV, *Native* plasma membrane vesicle fraction; MDA, *N*-methyl-D-aspartate.

with the Declaration of Helsinki and with the 1998 Animal Act of Hungary. Materials used in the experiments included: the membrane-impermeant form of the fluorescent Ca^{2+} ion indicator, bis-FURA2 (Molecular Probes, Unilab, Budapest, Hungary); Glu, HEPES, aprotinin, leupeptin, antipain, pepstatin, phenylmethylsulfonyl fluoride, and butylated hydroxy-toluene (Sigma, Budapest, Hungary); $CaCl_2$, NaCl, KCl, $MgCl_2$, NaOH, and glucose (Fluka, Budapest, Hungary); *t*ACPD, (*S*)-AMPA, (*R*)-AMPA, CNQX, cyclothiazide, kainate, and MK-801 (Tocris-Cookson, Bristol, UK), [^{3}H]Glu (49 Ci/mmol) (Amersham Pharmacia Biotech, Vienna, Austria). *p*-Cresol of analytical grade (Reanal, Budapest, Hungary) applied in model hydrogen bonding experiments was vacuum-distilled (5 mm Hg, 76°C) before use. Analytical grade solvents $CHCl_3$ and CCl_4 were from Chemolab and Reanal (Budapest, Hungary), respectively. The ethanol content of $CHCl_3$ was removed by distillation, the analytical grade CCl_4 was kept over water absorbent molecular sieves (Klinosorb 4; Reanal, Budapest, Hungary).

Synthesis and Purification of QXs. Derivatives of 2-methyl-4-oxo-3*H*-quinazoline-3-alkyl-carboxylic acid were prepared as described earlier by Almási et al. (1999). Briefly, 4-oxo-3*H*-quinazoline was synthesized according to LeMahieu et al. (1983). Alkyl-carboxylic acid derivatives of 2-methyl-4-oxo-quinazoline, 3-acetic (Q1) and 3-propionic (Q2), were prepared as described by Errede and McBrady (1978). Methylester (Q3), diethylacetamide (Q4), piperidine (Q5), and morpholine (Q6) derivatives of Q1 were prepared according to Barthwal et al. (1973). The above compounds were purified with crystallization in ethanol followed by reversed-phase TLC, performed with the use of silanized, precoated silica gel $60F_{254}$ plates (Merck, Budapest, Hungary) developed with $MeOH/H_2O$ (55:45) solvent mixture. The Q5 derivative was purified further by applying to a silica gel 60 (70–230, mesh ASTM) column eluted with toluene/methanol (10:1) solvent mixture.

Preparation of NPMV Suspensions. Suspensions of NPMV containing resealed plasmalemmal fragments and nerve endings were prepared as described earlier (Kardos et al., 1994). Rats were sacrificed by decapitation with a guillotine. The cerebral cortex was homogenized (Ultra-Turrax T25; Janke and Kunkel IKA Labortechnik, Staufen Germany) in 30 ml of 10 mM HEPES-NaOH-buffered 0.32 mM sucrose solution containing protease inhibitors (1 mM phenylmethylsulfonyl fluoride; 0.01 mg/ml aprotinin; 0.005 mg/ml each antipain, leupeptin, pepstatin A), and antioxidant (butylated hydroxy-toluene, 0.02 mM), pH 7.5. Thereafter 30 ml of Ca^{2+}-HEPES buffer, containing 145 mM NaCl, 5 mM KCl, 1.2 mM $CaCl_2$, 1 mM $MgCl_2$, 10 mM glucose, and 20 mM HEPES adjusted to pH 7.5 with 6 mM NaOH, was added and the suspension was centrifuged at 270 *g* for 4 min at 4°C. The supernatant was centrifuged at 6500 *g* for 20 min at 4°C. The pellet was homogenized with a Potter-Elvehjem glass-Teflon homogenizer (20 strokes up and down by hand) in 60 ml of the above buffer and centrifuged at 4,500*g* for 15 min, at 4°C. The resulting pellet was resuspended in 30 ml of Ca^{2+}-HEPES buffer and kept stirred in ice. Aliquots of 1.7 ml were centrifuged at 10,000*g* for 3 min at 4°C, and the pellet was resuspended as above in 5.5 ml of HEPES buffer, prepared as above without Ca^{2+} ion added at pH 7.5. The protein concentration was adjusted to 0.3 mg/ml according to the Folin reagent method (Lowry et al., 1951). The suspension was preincubated for 5 min at 30°C and used immediately in the transmembrane Ca^{2+} ion flux measurements.

Stopped-Flow Measurements of the Transmembrane Ca^{2+} Ion Flux. The effects of QXs on the AMPA receptor function were determined in measurements of the transmembrane Ca^{2+} ion influx into NPMV (Kardos et al., 1999) to (*S*)-AMPA as described recently (Kovács et al., 2000). Transmembrane Ca^{2+} ion flux rates were followed by rapid mixing of NPMV in 75 μl of buffer with an equal volume of buffer solution containing 1 μM membrane-impermeant form of the fluorescence Ca^{2+} indicator bisFURA2 in the absence or presence of 0.1 mM (*S*)-AMPA and 0.01 mM cyclothiazide with or without the QX. Under these conditions, the decrease of the fluorescence intensity of bisFURA2, monitored at 500 nm with the use of a 260 to 390 nm excitation filter, corresponded to the influx of Ca^{2+} ion into NPMV. Fast mixing of the thermostated reactants (30.0 ± 0.1°C) was performed in a SF-61 DX2 stopped-flow/UV Fluorescence Detection System (Hi-Tech Scientific, Salisbury, Wiltshire, UK), supported by the KinetAsyst2 software (Hi-Tech). The percentage fluorescence intensity in the period of 0.04 to 10 ms was recorded on a logarithmic base. Traces represent averages of 3 to 19 experiments. An experiment meant seven measurements providing sets of 512 data points acquired automatically. Transformation of the percentage fluorescence data into the percentage change of fluorescence was performed with subtraction of the background trace measured without additives. Traces were plotted so that positive values represent the influx of Ca^{2+} ion. The rate parameters for the agonist-induced transmembrane cation flux were determined by fitting the normalized percent change of fluorescence against time, measured in the absence or presence of various drugs, to the equation (Szárics et al., 2000):

$$F/F_{max} = 1 - \exp\{-[J_A(1 - \exp - \alpha t)/\alpha] + J_B[(1 - \exp - \beta t)/\beta] \quad (1)$$

where F/F_{max} is the fraction of Ca^{2+} ion flux that occurred at time t, J_A and J_B are the initial values of the first-order rate-constants for the Ca^{2+} ion flux; α and β are first-order rate constants for desensitization of the activities in the fast and slow phases. The rate constants were determined from the progress of transmembrane Ca^{2+} flux by fitting eq. 1. to data. Fitting, carried out by a nonlinear least-squares computer program using a modified Powell algorithm (Scientist version 2.0; MicroMath Inc., Salt Lake City, UT) provided the rate parameters with their standard deviations. Free fitting of data with rate parameters allowed to float from -∞ to +∞ was applied. The fast- and slow-phase responses were expressed as J_A/α and J_B/β.

[^{3}H]Glu Binding. For [^{3}H]Glu binding, aliquots of NPMV suspension in buffer containing 145 mM NaCl, 5 mM KCl, 1 mM $MgCl_2$, 10 mM glucose, and 20 mM HEPES adjusted to pH 7.5 with 6 mM NaOH were incubated with equal amounts of buffered solution containing [^{3}H]Glu [final concentration, 2.7 nM (0.13 μCi/ml)] in the absence or (to define nonspecific binding) the presence of 10 μM CNQX for 20 min at 30°C. [^{3}H]Glu binding experiments were per-

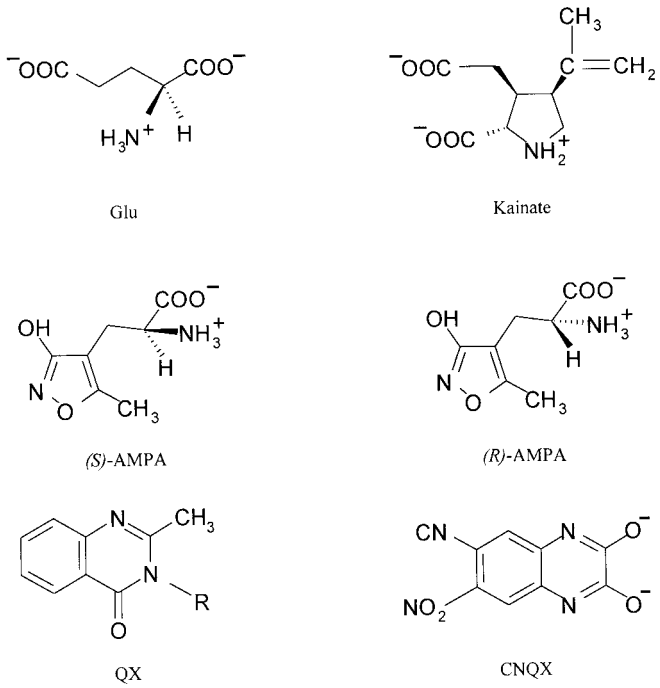

Fig. 1. Chemical structure of some iGluR agonists, antagonist and quinazolone-3-alkyl-carboxylic acid derivatives (QXs).

formed in the presence of 100 μM NMDA and the metabotropic Glu receptor agonist, *t*ACPD (50 μM). Samples of 500 μl were centrifuged at 10,000*g* for 3 min at 30°C. The supernatant of the samples was aspirated under vacuum and the pellets were rinsed three times with buffer. The radioactivity of the pellets was counted in "HiSafe" 3 (LKB, Uppsala, Sweden) scintillation mixture with an efficiency of 50%. Under the conditions, the nonspecific-to-total ratio of [^{3}H]Glu binding was 0.75.

The K_I constants for inhibition, defined as $K_I = IC_{50}/(1+\{[^3H]Glu\}/K_D)$, were determined from IC_{50} values obtained in measurements of displacement of specifically bound [^{3}H]Glu with different inhibitor concentrations varying in the range of 0.1 to 10 μM (Q1), 0.03 to 10 μM (Q2), 0.1 to 10 μM (Q5), 0.1 to 1000 μM [(*S*)-AMPA], 0.003 to 100 μM [(*R*)-AMPA], 0.03 to 10 μM (CNQX), 0.03 to 10 μM (Glu), 0.03 to 100 μM (kainate). Each displacement measurement, performed in duplicates, was repeated in seven [^{3}H]Glu binding experiments.

Docking Glu, Kainate, AMPA, CNQX, and QXs into the GluR2 Kainate-Binding Core. Molecular modeling using docking studies has been performed to explore favorable binding sites for a ligand in the GluR2 binding cavity. The GluR2 S1S2 protein coordinates (Protein Data Bank, code 1gr2), were determined by Armstrong et al. (1998) using the multiwavelength anomalous diffraction from crystals of the selenomethionine derivative of the rat GluR2 'flop' isoform polypeptide binding segments, S1S2, bound to the agonist kainate.

In the first step of the modeling studies it was checked whether the application of the DOCK procedure of the Sybyl 6.6 package by Tripos Inc. would lead to reasonable results for the S1S2-kainate complex. Water molecules (represented only by oxygen atoms in the original PDB file, thus hydrogens were generated) were saved and allowed to rotate and reposition. Their involvement in the ligand-binding turned out to be important. It has revealed from the calculations using the Tripos force-field and Gasteiger-Hückel charges, that the Thr103 and Arg108 residues of the S1 segment (abbreviated as S1/Thr103 and S1/Arg108, respectively) interact with the 2-carboxyl group of kainate. Furthermore, both attractive (between the 3-carboxyl methyl group of kainate and the S2/Ser158 and S2/Thr159 residues, and between the amino group of kainate and the S1/Pro101, S1/Thr103, and S2/Glu209 residues) and repulsive interactions (kainate with the S1/Tyr73) were observed. All these results are identical to those obtained by Armstrong et al. (1998) for the complex with kainate in the iGluR binding core; thus, the docking procedure was also considered a predictive methodology for systems with other ligands.

In these latter cases, the kainate molecule of the experimental complex was removed and either the AMPA or a QX ligand was positioned at its place in the binding pocket. Water molecules were saved in these calculations, as well. After minor manual adjustments for finding a favorable initial position for the ligand, the energy of the system was minimized throughout the docking procedure with fixed ligand geometry. In the final energy minimization, both elements of the complex were considered with flexible geometry. The docking procedure was somewhat modified for the rotational conformers of the ligands. Only one element of each mirror-image pair was placed in the original, unrelaxed protein environment at the onset of the calculations. The mirror-image counterpart was placed in the cavity formed by the relaxed protein structure, such as to mimic a change of the ligand conformation. The ligand binding energy, E_B, can be calculated as $E_B = E(RL) - E(R_{opt}) - E(L_{opt})$, where the terms stand for the energy of the optimized receptor-ligand complex, the isolated receptor and ligand, respectively (Huang et al. 1999). The first and third term can easily be evaluated using the Sybyl package, but finding the absolute minimum energy conformation for the receptor (R_{opt}) is practically impossible. Thus, binding energies of the L ligands relative to that of the kainate binding energy have been calculated in Table 3. In this case the $E(R_{opt})$ term is canceled as follows: $\Delta E_B = [E(RL) - E(L_{opt})] - [E\{(R)\text{-kainate}\} - E(\text{kainate}_{opt})]$. The results were represented with the interactive molecular graphics viewer, Rasmol. To facilitate the comparison, the essential amino acid residues of the ligand-binding core were aligned in the same positions by consistently using the same rotational and translational values in Figs. 3 and 4 (Sayle and Milner-White, 1995).

The equilibrium QXs geometries were obtained upon molecular-mechanics energy minimizations. For comparison, however, the Q1 structure was also studied using ab initio calculations (Q1b). The Q1b geometry was optimized at the HF/6-31G* level (Hehre et al., 1986) by using the Gaussian 94 package (Frisch et al., 1995) at the Ohio Supercomputer Center. Because each QX ligand is without a symmetry plane, there is always a pair of mirror-image conformers with equal energy. The gas-phase geometry of Q1 was obtained with the Sybyl software (Q1a). Q1a is nearly the mirror image of Q1b, indicating that the geometry of the most stable conformer determined by molecular-mechanics calculations and the far more sophisticated ab initio procedure is basically similar. The correspondence also suggests that the molecular-mechanics geometry optimization leads to reasonable results for the QX ligands.

The Q1 and Q2 ligands can take different protonation states depending on the environment (Almási et al. 1999). Gas-phase ab initio calculations for the Q1 ligand could not identify a locally stable zwitterionic structure. The geometry optimization led to a three-ring system (Q1c), with energy higher by 8.23 kcal/mol than Q1b at the MP2/6-31G*//HF/6-31G* level. This result indicates that the isolated zwitterionic Q1 is not stable. Interactions with a protein environment (including also water molecules in the binding pocket) however, may stabilize this tautomer. The ionization states of QXs were estimated by modeling the dynamics of the proton exchange in a protein-binding pocket containing water. To this end, proton magnetic resonance spectra (Varian Inova Unity 400 spectrometer, Varian, Palo Alto, CA) of the Q1 and Q2 ligands were recorded in a polar organic solvent, d_6-dimethyl sulfoxide, containing 0.01 M H_2O. These experiments indicated an abundance of the ionic side chain for the Q1 ligand (see under *Results*). Thus, the anionic and zwitterionic Q1 structures were also determined by Sybyl, and used in the docking studies along with the neutral Q2 and Q5 ligands.

Hydrogen Bonding Equilibrium between QXs and *p*-Cresol. Hydrogen bonding equilibrium between p-cresol and QXs was determined by applying infrared spectroscopic measurements in solution (Simonyi et al., 1976). Infrared spectra were recorded between 400 and 4000 cm^{-1} with 205 Fourier transform-IR single beam spectrophotometer (Thermo Nicolet, Madison, WI) in a 2.61-mm-wide NaCl cell by compensating for absorption bands caused by the solvent mixture applied (see below). To remove trace amounts of ethanol, QXs were dissolved first in a 1:1 mixture of dry CCl_4 and ethanol-free $CHCl_3$ and the solution was evaporated under vacuum (5 mm Hg). Thereafter, QXs were dissolved in the above mixture again and used in the measurements. Reference traces obtained with the QX tested (7.0 mM), were subtracted from spectra obtained in the presence of the QX (7.0 mM) with *p*-cresol (3.5 mM). The absorption peak height for the OH band of *p*-cresol was found at 3608 cm^{-1} in the above solvent mixture. Downward shifts in the OH band peak height ($\Delta\nu$ in cm^{-1}) were determined in the presence of the Q3, Q4, Q5, and Q6 and found $\Delta\nu$ = 185, 245, 228, and 201, respectively. The spectra of the carbonyl frequencies of the Q1, Q2, and Q5 (3.5 mM) were recorded in the absence (Q5) and presence (Q1 and Q2) of 0.1% dimethyl sulfoxide. Shifts of the CO frequencies of Q1 (1.7 mM), Q2 (2.0 mM), and Q5 (3.5 mM) as measured in the presence of 500 mM *p*-cresol were determined by subtracting the reference spectrum of *p*-cresol.

Results

A functional response of the AMPA receptor was assessed on the transmembrane Ca^{2+} ion influx to 0.1 mM (*S*)-AMPA with 0.01 mM cyclothiazide [an inhibitor of AMPA receptor

desensitization (Yamada, 1998)] in rat cerebrocortical homogenates containing resealed plasmalemma vesicles and nerve endings at 30°C. Two phases of Ca^{2+} ion influx with onsets of a few milliseconds and a few hundred milliseconds were distinguishable. The kinetic model (eq. 1.) accounted for almost all of the inward Ca^{2+} ion flux activity in the 0.1 ms to 10 s range of time (Fig. 2.). After the addition of 0.05 mM MK-801 [an antagonist of the NMDA receptor (Wong et al., 1986)] the inward Ca^{2+} ion flux activity to 0.1 mM (*S*)-AMPA increased rather than decreased. When both MK-801 (0.05 mM) and CNQX (0.01 mM) were present, the influx to 0.1 mM (*S*)-AMPA was blocked.

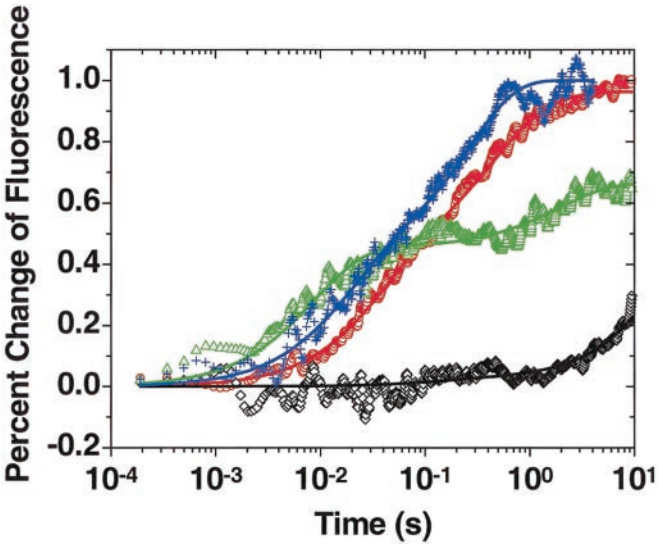

Fig. 2. Effects of 2-methyl-4-oxo-3*H*-quinazoline-3-acetic acid (Q1), 2-methyl-4-oxo-3*H*-quinazoline-3-propionic acid (Q2), and 2-methyl-4-oxo-3H-quinazoline-3-acetylpiperidine (Q5) on the rates of transmembrane Ca^{2+} ion flux to (*S*)-AMPA in suspensions of resealed plasmalemmal fragments and nerve endings from the rat cerebral cortex at 30°C. Symbols: 0.1 mM (*S*)-AMPA with 0.01 mM cyclothiazide, red circle; 0.1 mM (*S*)-AMPA with 0.01 mM cyclothiazide in the presence of 0.01 mM Q1, green triangle; 0.1 mM (*S*)-AMPA with 0.01 mM cyclothiazide in the presence of 0.01 mM Q2, blue cross; 0.1 mM (*S*)-AMPA with 0.01 mM cyclothiazide in the presence of 0.01 mM Q5, black diamond. The lines are computed by using eq. 1. for the rate parameters (1/s) $J_A = 11.2 \pm 0.2$, $\alpha = 21.4 \pm 0.7$, $J_B = 2.14 \pm 0.05$, $\beta = 0.78 \pm 0.02$ [(*S*)-AMPA]; $J_A = 55 \pm 2$, $\alpha = 91 \pm 3$, $J_B = 0.21 \pm 0.01$, $\beta = 0.43 \pm 0.04$ (Q1); $J_A = 23.7 \pm 1.5$, $\alpha = 49 \pm 6$, $J_B = 4.29 \pm 0.42$, $\beta = 0.59 \pm 0.33$ (Q2); $J_A = 0.17 \pm 0.05$, $\alpha = 7.1 \pm 2.6$, $J_B = 0.032 \pm 0.002$, $\beta = 0.03 \pm 0.02$ (Q5).

The fast-phase of the transmembrane Ca^{2+} ion influx to 0.1 mM (*S*)-AMPA with 0.01 mM cyclothiazide was inhibited completely by the presence of 0.01 mM Q5, whereas the inhibition of the slow-phase obeyed the Q1 > Q5 sequence (0.01 mM each, Fig. 1.). The quinazolone-3-propionic acid (Q2) and the quinazolone-3-acetic acid methylester (Q3) enhanced the slow-phase inward Ca^{2+} ion flux response to (*S*)-AMPA, whereas the diethylamino (Q4) and morpholino (Q6) derivatives of Q1 were found to be ineffective in both phases (Table 1).

The CNQX-displaceable [^{3}H]Glu binding (as measured in the presence of saturating concentrations of NMDA and *t*ACPD) revealed that Q1, Q2, and Q5 bound to this agonist site with medium affinity (Table 2). The rank order of inhibition of specifically bound [^{3}H]Glu by QXs was Q2 > Q1≈Q5 with maximal displacements of 100, 30, and 60%, respectively. The pharmacological profile of [^{3}H]Glu binding showed high affinity for (*R*)-AMPA (14 nM) and medium affinity for (*S*)-AMPA (0.21 μM), CNQX (0.31 μM), Glu (0.37 μM), and kainate (0.69 μM). Displaying the Q2 > (*R*)-AMPA > (*S*)-AMPA sequence, Q2, (*R*)-AMPA, and (*S*)-AMPA inhibited specific [^{3}H]Glu binding with low affinity as well (Table 2).

Docking ligands into the binding core altered both the optimized initial conformations of the ligands (Fig. 3.) and the unoccupied binding core formed by the amino acid residues of S1 and S2 polypeptide segments to various extent (Table 3; Fig. 4.). Mutual changes are consequences of net-attractive nonbonded interactions and H-bonds between amino acid residues of the iGluR binding pocket and the ligands. In addition to classical H-bonds between proton donor groups (OH or NH) and electronegative atoms (O or N) (Pimentel and McClellan, 1960), we examined H-bond-type interactions of groups XH (X = O, N) and CH with p (XH/p)

TABLE 1

Effects of quinazolone-alkylcarboxylic acid derivatives (0.01 mM) on the fast- and slow-phase Ca^{2+} ion permeability responses of AMPA receptors in suspensions of resealed plasmalemmal fragments and nerve endings from the rat cerebral cortex at 30°C

Values were rounded to the closest decimal number.

Additives		Functional Response			
		Fast-Phase		Slow-Phase	
		J_A/α	J_A/α (%)	J_B/β	J_B/β (%)
(*S*)-AMPA	None	0.5	100	2.7	100
(*S*)-AMPA	Q1—R: —CH_2COOH	0.5	100	0.5	20
(*S*)-AMPA	Q2—R: —$(CH_2)_2COOH$	0.5	100	7.3	270
(*S*)-AMPA	Q3—R: —CH_2COOCH_3	0.5	100	5.7	210
(*S*)-AMPA	Q4—R: —$CH_2CON(C_2H_5)_2$	0.5	100	2.7	100
(*S*)-AMPA	Q5—R: 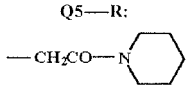	0.0	0	1.1	40
(*S*)-AMPA	Q6—R: 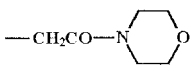	0.5	100	3.3	120

TABLE 2

Displacement of specifically bound [^{3}H]Glu to rat cerebrocortical NPMV suspensions at 30°C

Maximal displacements of specifically bound [^{3}H]Glu by Q1 and Q5 were 30% and 60%, respectively.

Ligands	Specifically bound [^{3}H]Glu(K_I)
	K_i(μM)
Q1	0.30 ± 0.10
Q2	0.10 ± 0.07 and 2.0 ± 0.5
Q5	0.30 ± 0.15
(*S*)-AMPA	0.21 ± 0.11 and 100 ± 34
(*R*)-AMPA	0.014 ± 0.008 and 10 ± 4
CNQX	0.31 ± 0.05
Glu	0.37 ± 0.11
Kainate	0.69 ± 0.27

and lone pair electrons (CH/n) (Nishio et al., 1998) together with the weak H-bond-type secondary attraction between CH and p electrons of (CH/p; Nishio et al., 1998). Water molecules sequestered nearby the ligands were taken into account, as well.

The oxo-isoxazole tautomer of the (*S*)- and the (*R*)-AMPA zwitterion participated in multiple contacts with residues from both segments (Tables 3 and 4, Fig. 4.). Interaction of the oxo-isoxazole (*S*)-AMPA zwitterion with Tyr73 was found to be unique with respect to the follow-up interaction of Tyr73 with Glu25. Instead, the docked oxo-isoxazole (*R*)-AMPA zwitterion showed H-bond interaction between Glu25 and Thr190 (Table 3).

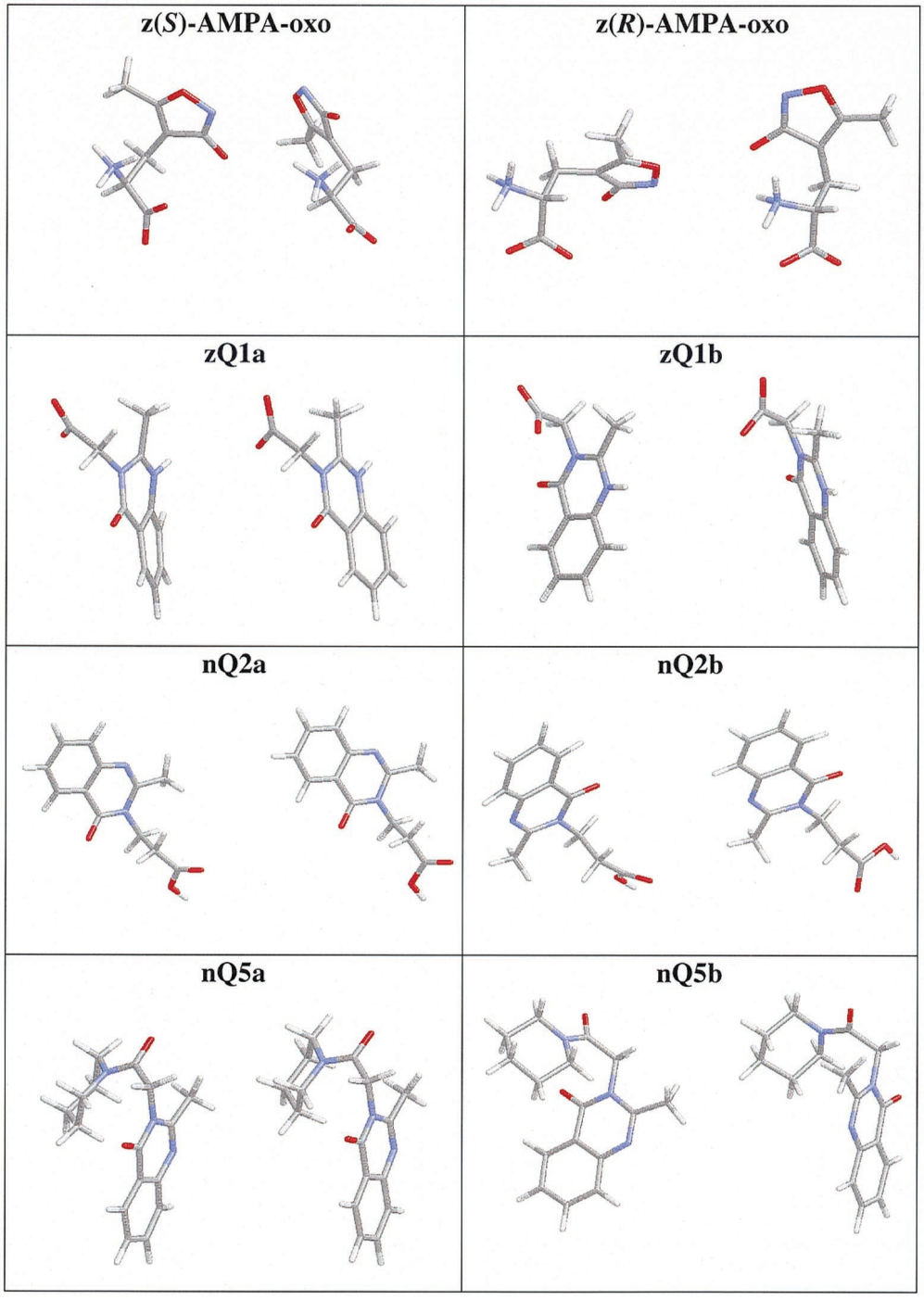

Fig. 3. Docked (right) and initial (left) optimized conformations of various models of AMPA and QX ligands: zwitterionic oxo-isoxazole tautomer of (*S*)- and (*R*)-AMPA [z(*S*)-AMPA-oxo and z(*R*)-AMPA-oxo], mirror-image pairs of zwitterionic 2-methyl-4-oxo-3*H*-quinazoline-3-acetic acid (zQ1a and zQ1b), 2-methyl-4-oxo-3*H*-quinazoline-3-propionic acid (nQ2a and nQ2b), and 2-methyl-4-oxo-3*H*-quinazoline-3-acetylpiperidine (nQ5a and nQ5b).

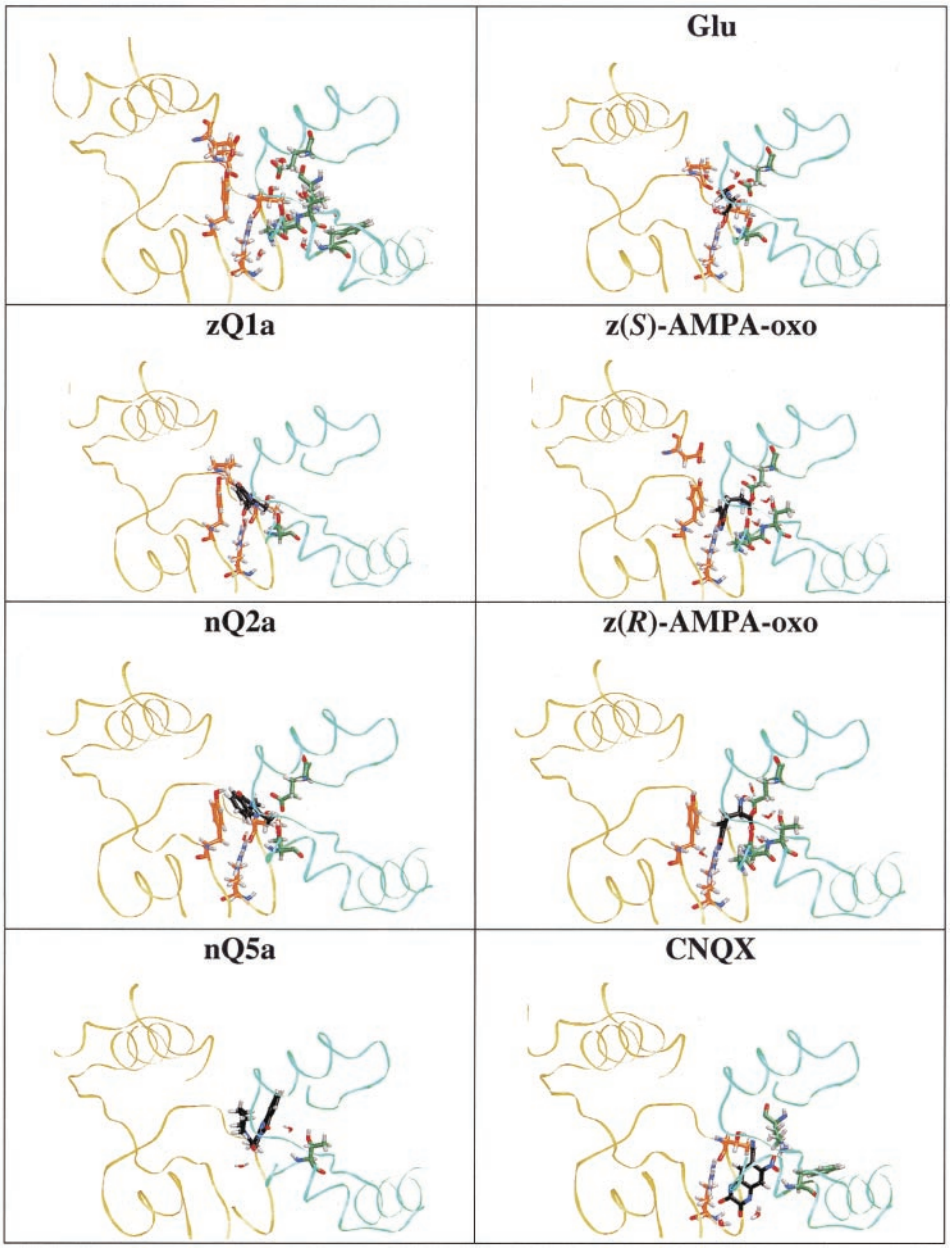

Fig. 4. Views of zGlu, 2-methyl-4-oxo-3*H*-quinazoline-3-acetic acid (zQ1a), z(*S*)-AMPA-oxo, 2-methyl-4-oxo-3*H*-quinazoline-3-propionic acid (nQ2a), z(*R*)-AMPA-oxo, 2-methyl-4-oxo-3*H*-quinazoline-3-acetyl piperidine (nQ5a), and CNQX bound in the interdomain crevice of the GluR2 subunit (none), showing interacting amino acid residues. S1 segment, orange; S2 segment, green. z, zwitterion; *n*- neutral; a, anionic; oxo, oxo-isoxazole AMPA tautomer.

TABLE 3
Changes in the minimal distance of attractive interactions within 2.5 Å between selected pairs of amino acid residues constituting the iGluR binding core

Ligands	Glu25 Thr190	Lys72 Asp155	Tyr73 Glu25	Thr103 Arg108	Thr103 Glu209
			2.1	2.1	2.0
zGlu	1.8	1.6		1.8	1.7
zKainate		1.6		1.8	1.6
z(*S*)-AMPA-oxo		1.6	1.7	1.8	1.7
z(*R*)-AMPA-oxo	1.9	1.6		1.7	1.8
CNQX		1.6		1.7	
aQ1a		1.6		1.7	1.7
aQ1b		1.6		1.7	1.8
zQ1a		1.6		1.7	1.7
zQ1b		1.6		1.7	1.7
nQ2a		1.7		1.8	1.7
nQ2b		1.6		1.7	1.8
nQ5a		1.7		1.7	1.7
nQ5b		1.7		1.7	1.7

z, zwitterion; n, neutral; a, anionic; oxo, oxo-isoxazole AMPA tautomer.

The Q1 proton magnetic resonance spectrum showed extremely fast exchange between the protons of the carboxyl group and H_2O, indicating that the anionic form of Q1 was abundant. The simultaneous appearance of the 12.50 ppm band for the acidic proton and the narrow H_2O band at 3.31 ppm showed Q2 to be un-ionized. Thus, besides the neutral mirror-images nQ1a, nQ1b (and nQ1c), the anionic (aQ1a and aQ1b) and zwitterionic (zQ1a and zQ1b) models of Q1 (Table 3 and Table 4, Fig. 4.) were also docked. All docked Q1 models did show a smaller number of associations to S2-segment amino acid residues than the (*S*)-AMPA ligand, whereas H-bond interactions coupling the S1-segment amino acid residues with the ionic Q1a models were more abundant than those for (*S*)-AMPA. When docked, the neutral Q2a conformer showed associations to S1/Tyr73, S1/Arg108 and S2/Ser158, S2/Glu209 (Table 4, Fig. 4.). None of the docked conformers of the neutral Q5 ligand approached the S1- and S2-segment amino acid residues within 2.5 Å (Table 4, Fig.

4.). Docking indicated H-bond formation between the OH group of S1/Tyr73 and the lactam carbonyl group of some QX models (compare Q1 and Q2 in Fig. 4. and Table 4). These interactions were studied by IR measurements for model systems consisting of a QX ligand and *p*-cresol. In the presence of *p*-cresol, the lactam C═O band of Q1 and Q2 showed a downward shift of $\Delta\nu > 40$ (cm^{-1}). By contrast, the OH group in *p*-cresol interacted with the side chain amide C═O of the Q5 derivative as indicated by its downward shift of $\Delta\nu$=11 (cm^{-1}).

Relative binding energies in Table 4 show stronger binding for the AMPA enantiomers than for kainate. The stabilization is very large, about −65 kcal/mol without noteworthy difference for the *R*- and *S*-configurations. For all QX ligands, the relative binding energy is positive. In these cases, however, stereochemical factors are important. All QXa structures bind more strongly than the QXb conformers; binding of ligands with ionic side chain is preferred over the neutral forms. The anionic ligand binds more strongly than the zwitterionic one, as seen from a comparison of the values for aQ1 and zQ1. Orientation of the ligand side chain, however, is so important that a zwitterionic Q1a ligand can become more appreciated by the receptor than an anionic Q1a conformer: the E_B values for zQ1a and aQ1b are 11 and 32 kcal/mol, respectively.

The large, 8- to 21-kcal/mol increase in the binding energy disfavors formation of the nQ2b and nQ5b conformations of the ligands in their bound form. This encounter seems to occur due to the receptor environment. Low rotational barriers, 2.3 and 3.5 kcal/mol, were calculated for the isolated neutral Q2 and Q5 structures, respectively. The rotational barriers for the neutral, anionic, and zwitterionic Q1 ligand are 3.7, 9.0, and 9.9 kcal/mol, respectively. The latter two values are still too small compared with the binding energy increase of 25 and 43 kcal/mol, following the conformational changes of the bound aQ1 and zQ1 ligands, respectively.

Comparison of the E_B values and the numbers of the hydrogen bonds in Table 4 suggests that the ligand is mainly stabilized by formation of hydrogen bonds. The intermolecular van der Waals interaction energy may change only slightly upon rotation of the ligand side chain. Formation of hydrogen bonds to the receptor is feasible, however, only in some specific ligand conformation. Table 4 suggests that the Q1a and Q2a conformers fit better in the receptor binding pocket than the corresponding "b" conformers. Based on the results in the table, hydrogen bonds to Thr103 and Arg108 are developed in the "a" conformation. No such bonds have been observed for Q1b and Q2b, which explains, at least partially, the difference in E_B. Number and strength of the hydrogen bonds are not, however, the only factors that determine the binding energy. Indeed, the nQ5 ligand binds more strongly than nQ2 despite the larger number of hydrogen bonds formed by the latter. The Q5 ligand has a bulkier side chain that can be more favorably stabilized by van der Waals interactions than the smaller Q2. Thus, we may conclude that the binding energies for the QX ligands have been calculated as a delicate balance of the electrostatic, H bond, and van der Waals interactions.

Discussion

The Ca^{2+} ion permeability response to (*S*)-AMPA observed in rat cerebrocortical membranes could be the result of membrane depolarization raising Mg^{2+} ion blockade of the NMDA receptor (Turecek et al., 1997). However, the presence of an NMDA receptor antagonist (MK-801) does not inhibit, but instead enhances the inward Ca^{2+} ion flux to (*S*)-AMPA, displaying CNQX sensitivity. Enhanced Na^+ ion translocation (Szárics et al., 2000) and $^{22}Na^+$ ion exchange (Serfozo and Cash, 1995) in NPMV suspensions from the rat hippocampus mediated by 0.1 mM Glu in the presence of 0.05 mM MK-801 was documented previously. Thus, the inward Ca^{2+} ion flux to (*S*)-AMPA observed in rat cerebrocortical NPMV suspensions was identified with the Ca^{2+} ion permeability response of AMPA preferring receptor(s).

Comparisons made between the kinetics of the inward Ca^{2+} ion flux to (*S*)-AMPA in cerebrocortical homogenates and that of the transmembrane Na^+ ion influx mediated by an AMPA receptor in hippocampal homogenates (Szárics et al., 2000) have established that the agonist-induced opening of the AMPA receptor channels occurs in two, kinetically distinguishable, phases. Here we report that the 2-methyl-4-oxo-3*H*-quinazoline-3-acetic acid (Q1) inhibits the slow-phase response specifically, whereas the acetyl piperidine deriva-

TABLE 4

The relative binding energy, E_B, kcal/mol, and number of favorable interactions found within 2.5 Å between different models of ligands in complex with amino acid residues constituting the iGluR binding core and tethered water molecules (W)

H-bond interactions between polar groups are indicated in bold.

Ligands	E_B	W	S1				S2			
			Tyr 73	Pro 101	Thr 103	Arg 108	Gly 157	Ser 158	Thr 159	Glu 209
zGlu	−28	**4**		**1**	**2**	**2**		**1**		**11**
zKainate	0	**4**		**1**	**1**	**2**		**1**	**2**	**1**
z(*S*)-AMPA-oxo	−65	**4**	1			**1**	1	**2**	**1**	**2**
z(*R*)-AMPA-oxo	−64	**4**	1			**2**	2	1	**1**	**1**
CNQX	−69	**2**			**1**	**1**				
aQ1a	7	**1**	**1**	1	**1**	**2**		1		
aQ1b	32	**2**	**1**					1		
zQ1a	11	**1**	**1**	1	**1**	**2**		1		
zQ1b	54	**2**	**1**					1		
nQ2a	56	**1**	**1**		**2**	**1**		1		1
nQ2b	64	**2**	**1**							**1**
nQ5a	26	**2**								
nQ5b	47	**2**								

z, zwitterion; n, neutral; a, anionic; oxo, oxo-isoxazole AMPA tautomer.

tive (Q5) is a more potent inhibitor of the fast-phase response. Both the quinazolone-3-propionic acid (Q2) and the quinazolone-3-acetic acid methyl ester (Q3) enhanced the slow-phase response to (*S*)-AMPA.

Brain-derived membranes that contain large repertoire of multiple receptor subunits with several different subtypes have been used in this study. We propose that differences in receptor subunit compositions could explain the occurrence of cerebrocortical Ca^{2+} ion (observed in this study) and hippocampal Na^{+} ion-permeable (Szárics et al., 2000) AMPA preferring receptors with different lifetimes. Exploiting the distinguishable values of K_I constants for (*R*,*S*)-AMPA (0.01–0.04 μM), CNQX (0.13–0.46 μM), Glu (0.16–0.48 μM), and kainate (0.22–3.0.5 μM) determined by inhibition of specific [^{3}H](*R*,*S*)-AMPA binding to recombinant receptor subunits stably expressed in baby hamster kidney cells (Andersen et al., 1996), the presence of the iGluR1 (flip and flop), the iGluR4 (flip and flop) and the Ca^{2+} ion permeable GluR2**Q** (flip) subunits (Hollmann and Heinemann, 1994; Andersen et al., 1996) can be diagnosed in rat cerebrocortical NPMV suspensions. Identification of the Ca^{2+} ion impermeant GluR2**R** (Hollmann and Heinemann, 1994) in rat cerebrocortical NPMV suspensions is not feasible by its pharmacological profile; however, it might possibly be present as observed by its unique feature (Andersen et al., 1996) (i.e., the occurrence of a low-affinity agonist binding site). The presence of the flip and flop iGluR1 and iGluR4 together with the Ca^{2+} ion permeable GluR2**Q** (flip) subunits in cerebrocortical membranes suggests that (1) Ca^{2+} ion permeable AMPA preferring oligomers are expressed in rat cerebral cortex, and (2) different subunit compositions correspond to kinetically distinguishable receptors, explaining the selectivity of Q1 for the long-lived and Q5 for the short-lived Ca^{2+} ion-permeable receptors. The exploitation of differences between these similar receptors will be important in the development and use of drugs with high pharmacological specificity. Since the closed ligand-binding core renders iGluR able to open (Paas et al., 2000), an enhancement of the AMPA preferring Ca^{2+} ion permeability response by Q2 and Q3 may possibly be activated by binding of these QXs to some other agonist or coagonist (like Gly in the case of NMDA receptor, Laube et al., 1997) sites.

Partial or total displacement of [^{3}H]Glu from specific, CNQX-sensitive agonist binding sites by Q1, Q5 or Q2, respectively, justifies the use of the X-ray crystal structure of the ligand-binding core of iGluR2. Now the question arises, how the ligand-receptor interaction, seen in the complex of iGluR S1S2 and QXs explains inhibition or enhancement of fast- and slow-phase AMPA receptor responses. The fast- and the slow-phase responses can be described as a result of variable degree or different mode of domain closure constituted by attractive noncovalent interactions between amino acid residues of the iGluR2 S1S2 binding core and the agonist.

Effective QX models may be selected upon the calculated relative binding energy from docking (Table 4). Thus, the ionic Q1a and the neutral Q5a should fit better than their mirror-images, suggesting that a strategy of chiral center incorporation by substitutions at side chain methylene position of QX ligands would possibly create more specific AMPA receptor antagonists. Note, however, that the downward shifts of relative binding energy from docking were found less predictive in case of the neutral Q2 mirror-images and in case of the functionally active and inactive enantiomers (Lauridsen et al., 1985) of AMPA. Obeying the CNQX ~ z(*S*)-AMPA-oxo ~ z(*R*)-AMPA-oxo > Glu > kainate > aQ1a ~ zQ1a > nQ5a > nQ2a sequence, the downward shift of relative binding energy from docking does not predict the AMPA receptor permeability response to these ligands either. Remarkable entropy changes are also expected throughout the binding process, but these changes cannot be followed at the present level of modeling. The $\Delta G = \Delta H - T\Delta S$ free energy change of the process, which defines the binding constant, is not expected to be as large as the binding energy change. The energy and entropy contributions are of opposite sign in many cases, thus large absolute value energy and entropy changes can lead only to small changes in ΔG. Hydrogen-bond formation decreases the total system energy but also reduces the entropy upon reduced torsional, rotational ability of the bonds involved. Strong binding of solvent molecules decreases the energy of the system, but the entropy is also decreased in a more ordered system.

Thus, the relative binding energy from docking may not have relevance to the pharmacological (agonistic or antagonistic) specifics of the AMPA receptor ligands considered. These specifics were approximated based on variable degree of S1S2 bridging interactions between the ligands and the amino acid residues of the iGluR S1S2 binding core. A comparison of the S1S2 bridging interactions of Q2 and (*S*)-AMPA with their effects on the AMPA receptor permeability responses suggests that the quinazolone-3-propionic acid may facilitate the slow-phase permeability response of the AMPA receptor, if two S1S2 bridging interactions involving Tyr73, Arg108, Ser158, and Glu209 were considered both necessary and sufficient for constituting agonist-induced domain closure with the AMPA receptor. The pattern obtained with the docked ionic Q1 models explained how the quinazolone-3-acetic acid, which induces a single S1S2 bridging interaction, could function as a specific inhibitor of the slow-phase permeability response of the AMPA receptor. The lack of S1S2 bridging interactions seen in complex of iGluR2 S1S2 and Q5 explains why quinazolone-3-acetyl-piperidine could function as an inhibitor of both phases of AMPA receptor response.

The residue at position 190 of iGluR2 S2 polypeptide segment in the kainate receptors GluR5 and GluR6 was found important in determining sensitivity to AMPA (Swanson et al., 1997). As seen with functionally inactive enantiomer, (*R*)-AMPA, the OH group of Thr190 forms an H bond with Glu25. Disruption of this interdomain interaction occurred because of H bond interaction between Glu25 and Tyr73 contacted by the functionally active (*S*)-AMPA enantiomer, suggests that the control of the permeability response of the AMPA receptor may also occur through allosteric interactions involving residue pairs Tyr73-Glu25 and Glu25-Thr190.

Acknowledgments

P.I.N. thanks the OHIO Supercomputer Center for the computer time used in the quantum chemical calculations.

References

Almási J, Takács-Novák K, Kökösi J and Vámos J (1999) Characterization of potential NMDA and cholecystokinin antagonists II. Lipophilicity studies on 2-methyl-4-oxo-3H-quinazoline-3-alkyl-carboxylic acid derivatives. *Int J Pharm* **180:**13–22.

Andersen PH, Tygesen CK, Rasmussen JS, Soegaard-Nielsen L, Hansen A, Hansen K, Kiemer A and Stidsen CE (1996) Stable expression of homomeric AMPA-selective glutamate receptors in BHK cells. *Eur J Pharmacol* **311:**95–100.
Armstrong N, Sun Y, Chen G-Q and Gouaux E (1998) Structure of a glutamate receptor ligand-binding core in complex with kainate. *Nature (Lond)* **395:**913–917.
Barthwal JP, Tandon SK, Agarwal VK, Dixit KS and Parmar SS (1973) Relationship between CNS depressant enzyme inhibitory properties of substituted quinazolone 1,3,4-oxadiazoles. *J Pharm Sci* **62:**613–617.
Errede AL and McBrady JJ (1978) Acylanthranys. 7. Influence of the end group on selectivity in the reaction of ω-substituted linear aliphatic amines with acetylanthranyl. *J Org Chem* **43:**1884–1887.
Frisch MJ, Trucks GW, Schlegel HB, Gill PMW, Johnson BG, Robb MA, Cheeseman JR, Keith T, Petersson GA, Montgomery JA, et al. (1995) *Gaussian 94, Revision E*. 2 Gaussian Inc, Pittsburgh.
Hehre WJ, Radom L, Schleyer PvR and Pople JA (1986) *Ab Initio Molecular Orbital Theory*. Wiley, New York.
Hollmann M and Heinemann S (1994) Cloned glutamate receptors. *Annu Rev Neurosci* **17:**31–108.
Huang XP, Nagy PI, Williams FE, Peseckis SM and Messer WS Jr (1999) Roles of threonine 192 and asparagine 382 in agonist and antagonist interactions with M_1 muscarinic receptors. *Br J Pharmacol* **126:**735–745.
Kardos J, Kovács I, Blandl T and Cash DJ (1994) Modulation of GABA flux across rat brain membranes resolved by a rapid quenched incubation technique. *Neurosci Lett* **182:**73–76.
Kardos J, Kovács I, Szárics É, Kovács R, Skuban N,Nyitrai G, Dobolyi Á and Juhász G (1999) Uridine activates fast transmembrane Ca^{2+} ion fluxes in rat brain homogenates. *Neuroreport* **10:**1577–1582.
Kovács I, Szárics É, Skuban N and Kardos J (2000) Deramciclane inhibits *N*-methyl-D-aspartate receptor function. *Brain Res Bulletin* **52:**39–44.
Laube B, Hirai H, Sturgess M, Betz H and Kuhse J (1997) Molecular determinants of agonist discrimination by NMDA receptor subunits: Analysis of the glutamate binding site on the NR2B subunit. *Neuron* **18:**493–503.
Lauridsen J, Honoré T and Krosgaard-Larsen (1985) Ibotenic acid analogues. Synthesis, molecular flexibility, and in vitro activity of agonists and antagonists at central glutamic acid receptors. *J Med Chem* **28:**668–672.
LeMahieu AR, Carson M, Nason CW, Parrish RD, Welton FA, Baruth WH and Yaremko B (1983) (E)-3-(4-oxo-4H-quinazoline-3yl)-2-propenoic acids, a new series of antiallergic agents. *J Med Chem* **26:**420–425.
Lowry OH, Rosebrough NJ, Farr AL and Randall RJ (1951) Protein measurement with the Folin phenol reagent. *J Biol Chem* **193:**265–275.
Nishio M, Hirota M and Umezawa Y (1998) *CH/p Interaction. Evidence, Nature, and Consequences* (Methods in Stereochemical Analysis series, Marchand AP ed) p. 2. Wiley-VCH, New York.
Paas Y (1998) The macro- and microarchitectures of the ligand-binding domain of glutamate receptors. *Trends Neurosci* **21:**117–125.
Paas Y, Devillers-Thiéry, Teichberg VI, Changeux J-P, Eisenstein M (2000) How well can molecular modeling predict crystal structure: The case of the ligand-binding domain of glutamate receptors. *Trends Pharmacol Sci* **21:**87–92.
Pimentel GC and McClellan (1960) *The Hydrogen Bond*, p 224, Freeman, San Francisco.
Sayle RA and Milner-White EJ (1995) Rasmol: Biomolecular graphics for all. *Trends Biol Sci* **20:**374.
Serfozo P and Cash DJ (1995) Glutamate receptor (a-amino-3-hydroxy-5-methyl-4-isoxazole propionate and kainate subtype) activity enhanced by dizocilpine (MK801) in rat hippocampus. *Eur J Biochem* **228:**498–505.
Simonyi M, Kovács I, Kardos J and Holly S (1976) Determination of the equilibrium constant of hydrogen bonding between substituted h-(d)-phenols and vinyl acetate in CCl_4 by i.r. measurements. *Spectrochim Acta A Mol Biomol Spectrosc* **32A:** 1387–1392.
Szárics É, Nyitrai G, Kovács I and Kardos J (2000) Kinetically distinguishable AMPA-Kainate receptors in rat hippocampus are associated with the loss of glutamate-sensitive conformational transitions. Stopped-flow measurements of Na^+ ion flux and receptor desensitization with *native* membrane. *Neurochem Int* **36:**83–90.
Swanson GT, Gereau RW IV, Green T and Heinemann SF (1997) Identification of amino acid residues that control functional behaviour in GluR5 and GluR6 kainate receptors. *Neuron* **19:**913–926.
Turecek R, Vlahová V and Vyklicky L Jr (1997) Spontaneous openings of NMDA receptor channels in cultured rat hippocampal neurons. *Eur J Neurosci* **9:**1999–2008.
Wong EH, Kemp JA, Priestley T, Knight AR, Woodruff GN and Iversen LL (1986) The anticonvulsant MK801 is a potent N-methyl-D-aspartate antagonist. *Proc Natl Acad Sci USA* **83:**7104–7108.
Yamada KA (1998) AMPA receptor activation potentiated by the AMPA modulator 1-BCP is toxic to cultured rat hippocampal neurons. *Neurosci Lett* **249:**119–122.

Send reprint requests to: Dr. Julianna Kardos, Department of Neurochemistry, Institute of Chemistry, Chemical Research Center, Hungarian Academy of Sciences, Pusztaszeri út 59–67. H-1025 Budapest, Hungary. E-mail: jkardos@cric.chemres.hu